JOURNAL OF GEOPHYSICAL RESEARCH, VOL. 103, NO. B10, PAGES 24,411–24,426, OCTOBER 10, 1998

# Earthquake triggering by transient and static deformations

J. Gomberg

U.S. Geological Survey, Center for Earthquake Research and Information, University of Memphis, Memphis, Tennessee

N. M. Beeler and M. L. Blanpied

U.S. Geological Survey, Menlo Park, California

P. Bodin

Center for Earthquake Research and Information, University of Memphis, Memphis, Tennessee

**Abstract.** Observational evidence for both static and transient near-field and far-field triggered seismicity are explained in terms of a frictional instability model, based on a single degree of freedom spring-slider system and rate- and state-dependent frictional constitutive equations. In this study a triggered earthquake is one whose failure time has been advanced by $\Delta t$ (clock advance) due to a stress perturbation. Triggering stress perturbations considered include square-wave transients and step functions, analogous to seismic waves and coseismic static stress changes, respectively. Perturbations are superimposed on a constant background stressing rate which represents the tectonic stressing rate. The normal stress is assumed to be constant. Approximate, closed-form solutions of the rate-and-state equations are derived for these triggering and background loads, building on the work of *Dieterich* [1992, 1994]. These solutions can be used to simulate the effects of static and transient stresses as a function of amplitude, onset time $t_0$, and in the case of square waves, duration. The accuracies of the approximate closed-form solutions are also evaluated with respect to the full numerical solution and $t_0$. The approximate solutions underpredict the full solutions, although the difference decreases as $t_0$ approaches the end of the earthquake cycle. The relationship between $\Delta t$ and $t_0$ differs for transient and static loads: a static stress step imposed late in the cycle causes less clock advance than an equal step imposed earlier, whereas a later applied transient causes greater clock advance than an equal one imposed earlier. For equal $\Delta t$, transient amplitudes must be greater than static loads by factors of several tens to hundreds depending on $t_0$. We show that the rate-and-state model requires that the total slip at failure is a constant, regardless of the loading history. Thus a static load applied early in the cycle, or a transient applied at any time, reduces the stress at the initiation of failure, whereas static loads that are applied sufficiently late raise it. Rate-and-state friction predictions differ markedly from those based on Coulomb failure stress changes ($\Delta$CFS) in which $\Delta t$ equals the amplitude of the static stress change divided by the background stressing rate. The $\Delta$CFS model assumes a stress failure threshold, while the rate-and-state equations require a slip failure threshold. The complete rate-and-state equations predict larger $\Delta t$ than the $\Delta$CFS model does for static stress steps at small $t_0$, and smaller $\Delta t$ than the $\Delta$CFS model for stress steps at large $t_0$. The $\Delta$CFS model predicts nonzero $\Delta t$ only for transient loads that raise the stress to failure stress levels during the transient. In contrast, the rate-and-state model predicts nonzero $\Delta t$ for smaller loads, and triggered failure may occur well after the transient is finished. We consider heuristically the effects of triggering on a population of faults, as these effects might be evident in seismicity data. Triggering is manifest as an initial increase in seismicity rate that may be followed by a quiescence or by a return to the background rate. Available seismicity data are insufficient to discriminate whether triggered earthquakes are "new" or clock advanced. However, if triggering indeed results from advancing the failure time of inevitable earthquakes, then our modeling suggests that a quiescence always follows transient triggering and that the duration of increased seismicity also cannot exceed the duration of a triggering transient load. Quiescence follows static triggering only if the population of available faults is finite.

## 1. Introduction

Triggering may be thought of as a hastening of the time of occurrence of inevitable earthquakes. This hypothesis underlies many recent studies and even earthquake forecasts [e.g., *Toda et al.*, this issue; *Nalbant et al.*, this issue; *Nostro et al.*, this issue]. It is also plausible that triggered earthquakes may be "new" [*Boatwright and Cocco*, 1996; *Gomberg et al.*, 1997]; that is, earthquakes that would not have happened in the absence of the triggering load. Like numerous other studies, we focus on the first hypothesis. Many of these studies show a positive



Paper number 98JB01125.
0148-0227/98/98JB-01125$09.00

correlation between the spatial distributions of aftershocks, or sequences of moderate to large events, with modeled changes in static Coulomb failure stresses (ΔCFS) generated by earlier nearby large earthquakes [*Stein and Lisowski*, 1983; *Reasenberg and Simpson*, 1992; *Harris and Simpson*, 1992, 1996; *Jaumé and Sykes*, 1992, 1996; *Stein et al.*, 1992; *King et al.*, 1994; *Harris et al.*, 1995; *Hodgkinson et al.*, 1996; *Nostro et al.*, 1997; *Deng and Sykes*, 1997; *Caskey and Wesnousky*, 1997; *Stein et al.*, 1997; *Pollitz and Sacks*, 1997]. These studies generally assume that all faults affected by the ΔCFS are truly locked during the interseismic period and fail when the stress on the fault reaches or exceeds a failure criterion given by $\tau_{\text{failure}} = C + \mu\sigma_n$, in which $\mu$ is the effective coefficient of friction, $\sigma_n$ is normal stress, $\tau_{\text{failure}}$ is shear stress at failure, and $C$ is the cohesion (Figure 1).

The most compelling spatial correlations between ΔCFS and triggered earthquakes appear to require time-dependent fault strength and/or an additional delaying mechanism because of the commonly observed delay between the triggering and triggered earthquakes [*Gomberg and Bodin*, 1994; *Harris*, this issue]. These observations are consistent with Coulomb failure if the static stress change brings a prestressed fault closer to (or farther from) failure, and the background tectonic loading simply finishes off the job: the triggered earthquake simply occurs ahead of schedule [*Harris and Simpson*, 1992; *King et al.*, 1994] by an amount referred to as the "clock advance" $\Delta t$ (Figure 1).

The simple Coulomb failure criterion does not account for all of the observations of triggered seismicity. Coulomb failure analysis only allows for delayed triggered seismicity to be induced by a change in the static stress field (Figure 1), whereas long-range interactions between earthquakes have been observed where static stress changes are negligible [*Kanamori*, 1972; *Rice and Gu*, 1983; *Newhall and Dzurisin*, 1988; *Keilis-Borok and Kossobokov*, 1990; *Kagan and Jackson*, 1991; *Hill et al.*, 1993, 1995; *Dieterich*, 1994; *Pepke et al.*, 1994; *Kossobokov and Carlson*, 1995; *Press and Allen*, 1995; *Protti et al.*, 1995; *Stark and Davis*, 1996; *Sturtevant et al.*, 1996; *Singh et al.*, 1998]. For example, the observation of widespread increases in seismicity (sometimes delayed) after the Landers earthquake, at distances where the static Coulomb stress changes were negligible, led many to consider the possibility that transient deformations (i.e., due to seismic waves) triggered the remote earthquakes [*Hill et al.*, 1993; *Anderson et al.*, 1994; *Gomberg and Bodin*, 1994; *Gomberg*, 1996]. The triggered sites have been shown to be uncorrelated statistically with regions of high heat flow [*Anderson et al.*, 1994]. Contrary to the assertion by some that transient triggering does not occur [*Scholz*, 1998], we suggest that such skepticism in part reflects observational difficulty of associating one earthquake with the passage of seismic waves from another, particularly if triggering is delayed. Indeed, triggering of earthquakes by man-made transient stress changes, albeit having longer duration than seismic waves, has long been accepted [*Raleigh et al.*, 1976; *Kisslinger*, 1976; *Simpson*, 1986; *Seeber et al.*, this issue].

The simple Coulomb failure model alone also does not explain the time-dependent nature of the failure threshold. For example, observations of repeated earthquakes for which the stress drop varies systematically with recurrence interval [*Kanamori and Allen*, 1986; *Scholz et al.*, 1986; *Vidale et al.*, 1994; *Marone et al.*, 1995] require that the failure strength increases with recurrence interval. These observations imply that the failure strength of faults depends on time and/or stressing rate. Related time-dependent effects are seen in studies of triggered seismicity where deformation changes (loads or, equivalently, stresses and strains) having a variety of time histories show that the failure threshold does not have a constant amplitude. Instead, triggering must depend on load amplitude, rate, and duration (i.e., it must be frequency-dependent). Evidence for this dependence comes from triggering of earthquake swarms at The Geysers, California, by some near and (large) distant earthquakes and by production of geothermal power, and from a lack of triggering by tidal stresses [*Gomberg and Davis*, 1996; *Vidale et al.*, this issue]. Existence of a triggering threshold that is a continuous function of frequency at The Geysers suggests that the same underlying physical process may apply regardless of the time history of the triggering load [*Gomberg and Davis*, 1996]. This further implies that the mechanism causing long-range triggering is neither extraordinary nor different from that causing static triggering at short distances.

Observational evidence indicates that the failure strength of faults in the Earth is not temporally or spatially constant. Therefore we adopt an alternative fault strength relation. We model the sensitivity of faults to triggered failure using a rate-and-state variable friction model. The rate-and-state variable equations [*Ruina*, 1983] were developed to characterize laboratory observations of fault friction and fault strength dependence on slip, time, and sliding velocity. Previous studies have found that fault models based on these relations reproduce many aspects of earthquakes and seismicity [*Dieterich*, 1979, 1981, 1986, 1994; *Rice and Gu*, 1983; *Gu et al.*, 1984; *Gu and Wong*, 1991, etc.]. An additional advantage to rate-and-state fault strength relationships is that the equations are related to known physical properties of the fault which likely influence the sensitivity of natural faults to triggered slip. These properties include the fault surface roughness [*Dieterich*, 1978, 1979], contact area [*Dieterich and Kilgore*, 1994], thickness of the gouge zone [*Marone and Kilgore*, 1993], and pore pressures and fluid flow [*Sleep and Blanpied*, 1992; *Sleep*, 1995, 1997; *Segall and Rice*, 1995]. Landers observations provide evidence that local physical characteristics and the orientation of a fault may exert primary influences on how it responds to applied deformations [*Anderson et al.*, 1994; *Spudich et al.*, 1995; *Gomberg*, 1996; *Gomberg and Davis*, 1996; *Gomberg et al.*, 1997]. The application of physically based rate-and-state frictional fault models to earthquake triggering should lead to increased understanding of the observations.

In this study, earthquakes are modeled as frictional instabilities of a massless slider block loaded by a spring. This physical system is analogous to a single fault patch of fixed dimensions that ruptures in an elastic medium [*Dieterich*, 1986, 1992] (Figure 2). The fault surface obeys rate-and-state friction and undergoes stick-slip failure when subjected to a constant background loading rate. To explore earthquake triggering, stress changes of two types are added to this background load: step increases, which represent coseismic static stress changes, and square wave "transients," which represent the passage of seismic waves. Numerical models of rate-and-state frictional systems show the square wave load to have similar effects on $\Delta t$ as an oscillating transient load [*Gomberg et al.*, 1997], the latter being most similar to seismic waves but the former being easier to deal with mathematically. These stress perturbations lead to triggered failure; in other words, they cause a change in the failure time, or clock advance $\Delta t$, relative to that observed for background loading alone. The potential for both static and transient loads to alter the timing of earthquakes is quantified

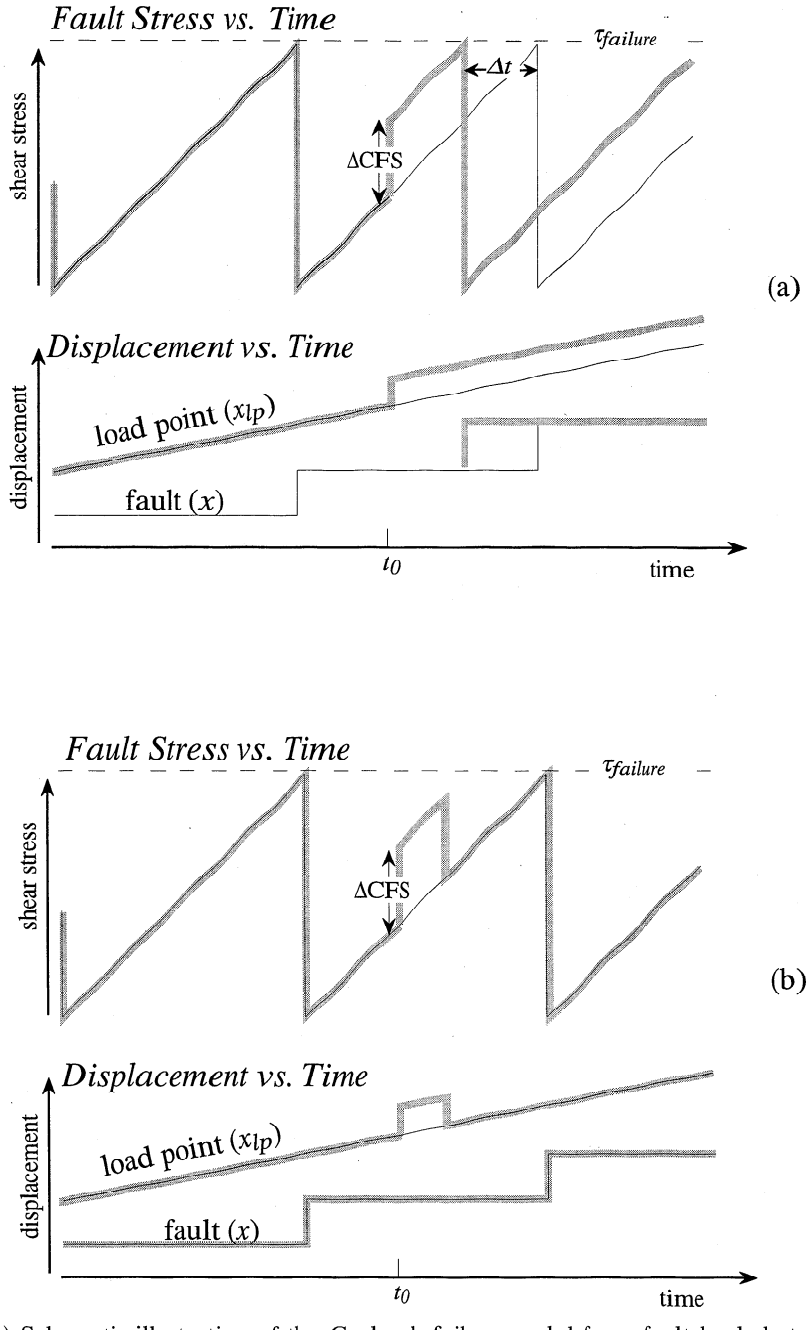


**Figure 1.** (a) Schematic illustration of the Coulomb failure model for a fault loaded at a constant background rate, $d\tau_b/dt$ (solid thin lines). Failure occurs when a threshold stress is reached and the accumulated stress is dropped. The cycle time is zeroed each time the stress drops. Although temporal changes in failure stress thresholds or stress drops are permitted in a Coulomb failure model, there is nothing in the underlying theory to explain how or why such changes would occur. Moreover, clock advances would result from changes in failure stress thresholds or stress drops and could not be distinguished from those attributed to ΔCFS. In other words, to be testable, models that associate ΔCFS with clock advance require a temporally constant failure stress threshold and stress drop. If a step function load with amplitude ΔCFS is added to the background at any time $t_0$ from the cycle start (shaded lines), the failure time is advanced by $\Delta t = \Delta\text{CFS}/(d\tau_b/dt)$. The fault remains locked (does not slip) until the failure stress threshold is reached. (b) The same Coulomb failure model as Figure 1a except that the triggering load is a square wave. Because the triggering load is transient and returns to the background only level, it does not cause a clock advance. If the transient load were large enough to reach $\tau_{\text{failure}}$, failure would occur during the transient and $\Delta t \approx t_f - t_0$.

by the development of approximate closed-form solutions to the rate-and-state equations for the cases of a single stress step (similar to those derived by *Dieterich* [1992, 1994]) and a single square wave transient. These solutions can be used to model earthquake triggering both in the near field where both static and transient deformations are of comparable magnitude and at remote distances where static deformations are negligible. We evaluate the accuracy of the closed-form solutions with

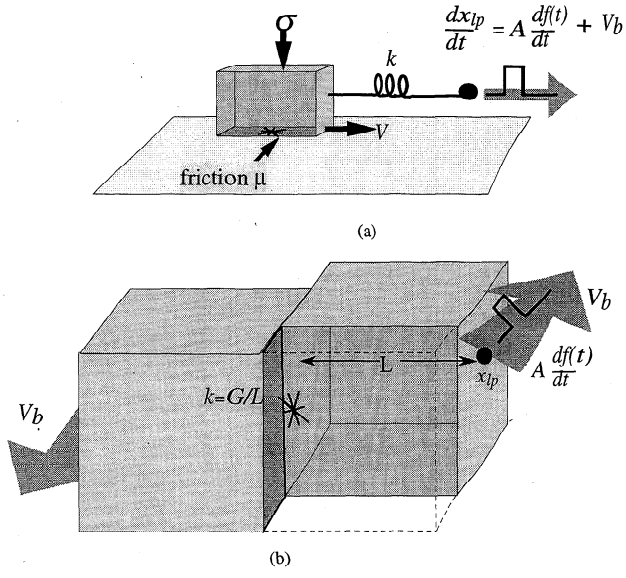


**Figure 2.** (a) Cartoon of our spring-slider model [from *Gomberg et al.*, 1997]. A constant normal stress $\sigma_n$ is applied to a massless block that sits on a frictional surface, connected to a spring with spring constant $k$. The load point $x_{lp}$ (solid dot) is displaced by loads that are applied with a constant "background" load velocity $V_b$ (large arrow) plus some additional triggering displacement load which has a time history described by $f(t)$ and amplitude $A$. In this study we use a simplified representation of seismic waves for which $f(t)$ equals a unit amplitude square wave, or a step function representing a coseismic static stress change. These loads cause the slider to move with velocity $V(t)$. (b) In the analogous fault model, two blocks of elastic material separated by a vertical fault (darker shading) undergo relative displacement (slip). Slip across the fault surface is driven from a load point at a distance $L$ with a fault-parallel constant velocity $V_b$ plus a triggering load described by $Af(t)$, resulting in a slip instability on the fault (asterisk). For a fault with fixed area the stiffness equals $G/L$ in which $G$ is the rigidity of the blocks.

respect to complete numerical calculations. Both the closed-form and numerical solutions are used to investigate the dependence of $\Delta t$ and stress at failure initiation on triggering load characteristics, particularly on when the triggering load is applied, $t_0$.

## 2. Model Formulation

We solve the rate-and-state equations numerically [also see *Gomberg et al.*, 1997] and also obtain approximate closed-form (analytical) solutions for $\Delta t$ associated with square-wave and step function triggering loads. Our analytic formulation extends that of *Dieterich* [1992, 1994] to explicitly consider the effect of a transient triggering load for a single earthquake source. The closed-form expressions provide direct insight into the response to both static and transient loads and enable us to calculate explicitly the effects of triggering load characteristics on the timing of subsequent earthquakes. The numerical calculations using the full rate-and-state equations allow us to determine the range of validity of the closed-form expressions. The numerical calculations also permit us to explore triggering responses beyond the range of validity of the closed-form expressions for a limited discrete set of parameters.

Frictional instability (stick-slip sliding) results when fault strength $\tau$ decreases more rapidly with slip $x$ than the elastic stiffness of the surroundings, $k = d\tau/dx$. Assuming that shear stress in the plane of the fault is proportional to normal stress $\sigma_n$ and assuming quasi-static motion, the friction is proportional to the difference between the load point displacement $x_{lp}(t)$ and slip on the fault $x(t)$ [*Dieterich*, 1981]:

$$\mu = \tau/\sigma_n = k[x_{lp} - x] \tag{1a}$$

or

$$d\mu/dt = k[dx_{lp}/dt - V] \tag{1b}$$

(Figure 2). Laboratory measurements show that fault friction is a function of time, slip, and slip velocity. These effects can be combined into one rate-and-state variable constitutive equation [*Ruina*, 1983]:

$$\mu(t) = \mu_0 + a \ln [V(t)/V_0] + b \ln [\xi(t)V_0/d_c]. \tag{2}$$

"Rate" refers to the (slider) velocity, $V = dx/dt$, or rate at which the fault slips. "State" $\xi$ is a function of time and slip and represents the physical properties of the fault surface or gouge (e.g., contact area or age, width of the deforming shear zone, porosity). Here $d_c$ represents a critical slip distance over which a population of contact points evolves, $a$ and $b$ are dimensionless empirically determined parameters, and $\mu_0$ and $V_0$ are a reference frictional coefficient and velocity, respectively. We also assume a constant normal stress $\sigma_n$ as in the studies of earthquake nucleation by *Dieterich* [1992] and *Roy and Marone* [1996], among others. State is described by [*Ruina*, 1983]

$$d\xi(t)/dt = 1 - \xi(t)V(t)/d_c \tag{3}$$

which requires that the fault ages and strengthens when stationary or is slipping slowly ($V \approx 0$, $d\xi/dt \approx 1$) as required by lab observations [*Dieterich*, 1972] and the existence of repeated earthquake sequences [*Brace and Byerlee*, 1966]. Equation (3) also implies that the fault weakens when slipping quickly ($V \gg 0$, $d\xi/dt < 0$), as in laboratory observations [*Okubo and Dieterich*, 1986] and theoretical considerations of failure [*Ida*, 1972; *Palmer and Rice*, 1972]. As the system approaches instability, the fault slip accelerates rapidly. As $V$ increases, $\xi$ decreases, allowing the fault to slip more easily.

We seek to derive a single closed-form expression for $V(t)$ for loads with different time functions. This is because closed-form expressions for $\Delta t$ are based on a failure criterion in which slip accelerates to high velocity. Recalling the assumption of quasi-static motion implicit in (1), we limit the scope of our study to the onset of rupture and failure, where inertial terms can be neglected. Building on the work of *Dieterich* [1992, 1994], we consider a general load displacement in (1),

$$x_{lp}(t) = V_b t + Af(t) + x_{init} \tag{4a}$$

$V_b$ is a constant "background" load velocity (e.g., that due to plate motions), $A$ is the amplitude of some additional triggering displacement load which has a time history described by $f(t)$, and $x_{init}$ is an initial displacement. Multiplying (4a) by the stiffness $k$ yields

$$\mu_{lp} = \dot{\mu}_b t + Bf(t) + \mu_{init}, \qquad B = Ak \tag{4b}$$

The rate at which shear stress grows due to background loading is described by $\dot{\mu}_b \sigma_n = (d\mu_b/dt)\sigma_n = kV_b\sigma_n$. $B\sigma_n$ is the peak shear stress of a triggering load, and $\mu_{init}\sigma_n$ is initial shear stress. The load point velocity is

$$dx_{lp}/dt = V_b + Adf(t)/dt \quad (4c)$$

For the numerical calculations the time derivatives of $\mu$, $\xi$, and $x_{lp}$ are calculated at each time step according to (1), (3), and (4c), respectively; $\mu$, $\xi$, and $x_{lp}$ are calculated at subsequent time steps using a Runga-Kutta algorithm, and $V$ and then $x$ are solved for using (2).

To derive the differential equation governing the evolution of displacement and thus of $V(t)$, we begin by substituting (4c) and (1) into the constitutive equation (2) and rearranging. This yields

$$V(t) = dx/dt = V_0 \exp\{[\mu(t) - \mu_0 - b \ln (V_0 t/d_c)]/a\}$$
$$= V_0 \exp\{[\dot{\mu}_b t + Bf(t) + \mu_{init} - kx - \mu_0 - b \ln (V_0 \xi/d_c)]/a\} \quad (5)$$

Following *Dieterich* [1992, 1994], the state evolution equation (3) has the approximate solution

$$\xi \approx \xi_{init} \exp[-x(t)/d_c] \quad (6)$$

when $V\xi/d_c \gg 1$. As will be shown, this approximation is only valid in the later portion of the earthquake cycle, as the slip accelerates toward failure. Using this approximate solution, (5) may be written as the differential equation

$$dx/dt = V_s \exp\{[\dot{\mu}_b t + Bf(t) + x(t)\gamma]/a\} \quad (7)$$
$$V_s = V_0 \exp\{[\mu_{init} - \mu_0 - b \ln (V_0 \xi_{init}/d_c)]/a\} \quad \gamma = (b/d_c - k),$$

in which starting conditions are embodied in the velocity $V_s$. In our numerical calculations, $\xi_{init}$ and $\mu_{init}$ are specified such that the initial stress or friction equals a fraction of the steady state value (see Table 1). In our closed-form solutions, $\xi_{init}$ and $\mu_{init}$ are set equal to values obtained from the numerical calculations at a time late in the cycle such that the approximation (equation (6)) is valid.

A general expression for the clock advance results from solving (7) by integrating according to

$$\int_0^x \exp\left[-\frac{\gamma x'}{a}\right] dx' = V_s \int_0^t \exp\left\{\frac{[\dot{\mu}_b t' + Bf(t')]}{a}\right\} dt' \quad (8)$$

**Table 1.** Parameters Used for Numerical and Appropriate Closed-Form Solution Calculations

| Parameter | Value |
|---|---|
| $a$ | 0.005 |
| $b$ | 0.010 |
| $\mu_0$ | 0.7 |
| $d_c$, m | 0.001 |
| $k/k_{crit}$ | 0.025 |
| $V_b = V_{ss}$, m/s | $10^{-10}$ |
| $V_0$, m/s | $10^{-10}$ |
| $V(t_0)$, m/s | $10^{-10}$ |
| $\mu(t_0)$ | $0.99\mu_{ss}$ |

In the numerical calculations, $\xi(t_0) = \xi_{init}$ is set so that the initial stress or friction equals $\mu(t_0)$. $V_{ss}$ is the sliding velocity when the system is at steady state. See *Gomberg et al.* [1997] for justification of this choice of values and associated references. (Note that a wide range of values are plausible, and these are simply one such set.) Initial conditions for analytic calculations are taken from numerical calculations, as indicated in corresponding figure captions. These values result in a background loading rate $d\tau/dt$ equal to 0.04 MPa/yr.

**Table 2.** Load Functions (Equation (10))

| Loading Type | Load Function $L$ |
|---|---|
| Background plus static (step) | $\exp(\dot{\mu}_b t_0/a)[1 - \exp(B/a)] - 1$ |
| Background plus transient (square wave) | $(\dot{\mu}_b t_w/a) \exp(\dot{\mu}_b t_0/a)[\exp(B/a) - 1] - 1$ |
| Background | $-1$ |

The time function $f(t)$ is easily defined for triggering loads imposed at onset time $t_0$. For the square wave of width $t_w$ it is

$$f(t) = 1 \quad t_0 < t < t_0 + t_w, \quad f(t) = 0 \quad \text{otherwise} \quad (9a)$$

or for a step it is

$$f(t) = 1 \quad t_0 < t, \quad f(t) = 0 \quad \text{otherwise} \quad (9b)$$

Using either (9a) or (9b) in (8), we integrate (8) to obtain an expression for the displacement expressed in a generalized form, valid for either square wave or step loads;

$$x(t) = -a/\gamma \ln\{1 - (V_s\gamma/\dot{\mu}_b)[\exp(B_{st}/a) \exp(\dot{\mu}_b t/a) + L]\} \quad (10a)$$

$L$ is a constant determined by what type of loading is applied (see Table 2) and is herein referred to as the load function. Note that $B_{st}$ in (10a) equals the amplitude of the step (i.e., $B_{st} = B$ for the step, and $B_{st} = 0$ otherwise) and is nonzero only for the step load.

Differentiating (10a) yields the velocity

$$V(t) = V_s \exp(B_{st}/a) \exp(\dot{\mu}_b t/a)/\{1 - (V_s\gamma/\dot{\mu}_b) \cdot [\exp(B_{st}/a) \exp(\dot{\mu}_b t/a) + L]\} \quad (10b)$$

We can now obtain a general expression for the clock advance by equating the velocities with and without any triggering load and solving for the time difference. While a clock advance can be defined using (10b), for any arbitrary choice of sliding velocity, we wish to determine the clock advance of the failure time. Here we define the time failure initiates as occurring when $V(t)$ becomes large, keeping in mind that because of the quasi-static assumption implicit in (1) we are required to consider this time as prior to the onset of dynamic motion. Hereafter, we use the term "failure" to refer to the initiation of failure as just defined (omitting "initiation of" for simplicity). This definition of failure is identical to that used by *Dieterich* [1992, 1994], and just as he does, we define the nominal failure time $t_f$ as the time of failure with only a background load ($B_{st} = 0$ and $L = -1$, Table 2) by solving (10b) for $V(t_f)^{-1} = 0$. The nominal failure time $t = t_f$ is [*Dieterich*, 1994]

$$t_f = (a/\dot{\mu}_b) \ln[1 + \dot{\mu}_b/V_s\gamma] \quad (11)$$

The difference between this failure time and one derived assuming a smaller velocity consistent with the quasi-static assumption is negligible (seconds relative to $\Delta t$ of the order of days or years) as long as $V$ at failure is much greater than the average long-term fault slip rate $V_b$ [*Dieterich*, 1994]. The time of failure when a triggering load perturbs the background, $t_p$, may be found similarly, using the appropriate load function $L$ (Table 2) and amplitudes $B$ and $B_{st}$. The clock advance is the difference between these, or

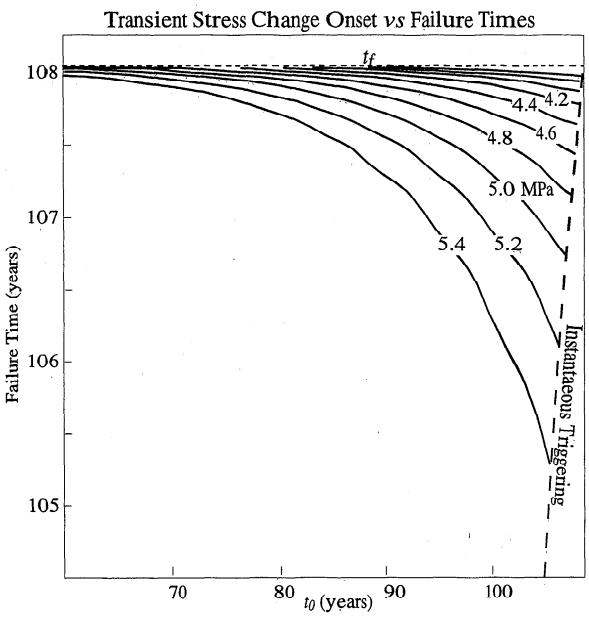


(a)

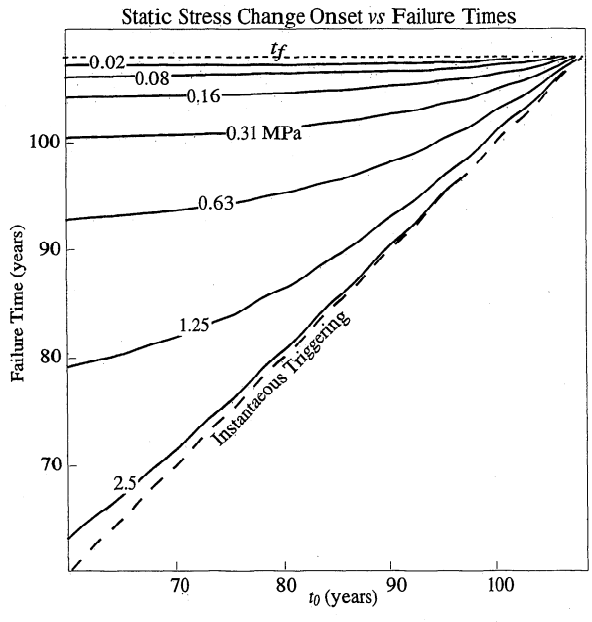


(b)

**Figure 3.** Calculations describing the relationship between time of instability and the time at which (a) a square wave of duration $t_w$ = 2000 s or (b) a step triggering load is applied, $t_0$. Curves show when instability occurs as a function of $t_0$, for a particular load amplitude (listed in megapascals on each line). In this example, in the absence of a triggering load, instability occurs at $t_f$ = 108.06 years (horizontal dashed line). Parameters used are listed in Table 1. The clock advance $\Delta t$ is the time interval (vertical distance) between a particular curve and $t_f$. Times of failure and clock advances were calculated using (12) and Table 2 and checked at several points using numerical calculations. The approximate calculations correctly predict the general features of the system responses, although the failure times are in error by a few percent when $t_0 \approx t_f$ and increase as $t_0$ decreases (see Figure 5). $V_s$ (equations (7) and (12)) is calculated using parameters in Table 1 and values of $\mu_{\text{init}}$ and $\xi_{\text{init}}$ estimated from the numerical solution at 108.0 years. Note the different vertical axis timescales for Figures 3a and 3b.

$$\Delta t = t_f - t_p = B_{st}/\dot{\mu}_b - a/\dot{\mu}_b \ln \{1 - [L + 1] \exp(-\dot{\mu}_b t_f/a)\} \quad (12)$$

Note that the term $B_{st}/\dot{\mu}_b = 0$ for the transient load.

An important implication of this rate-and-state model is that the total slip (upper displacement limit of the left-hand integral of (8)) is a constant for any given set of model parameters. As will be discussed in section 3, this implies a constant slip threshold for failure, in contrast to the stress threshold of Coulomb failure. To demonstrate the existence of a slip threshold, we note that for the slip at failure to be constant, the slip with a triggering plus background load, $x = x_p(t_p)$, must equal that for a background load only, $x = x_f(t_f)$, regardless of the loading history. For $x_f(t_f)$ to be equal to $x_p(t_p)$, from (10a) describing the displacement, the following equality must hold:

$$\exp(B_{st}/a) \exp(\dot{\mu}_b t_p/a) + L = -1 + \exp(\dot{\mu}_b t_f/a) \quad (13)$$

This is true because it is simply a restatement of (12) which was derived by equating velocities.

## 3. Frictional Instability Models

Much of the observational evidence for triggered seismicity cited in section 1 may be explained in terms of frictional instability, using numerical and/or approximate closed-form formulations. The examples we present are meant to illustrate the fundamental properties of these models, noting that the numbers obtained depend on the parameter values chosen (e.g., $d_c$, $a$, $b$). We use values consistent with previous studies (see *Gomberg et al.* [1997] for discussion and accompanying references). Equation (12) clearly shows that the clock advance $\Delta t$ depends on more than just the amplitude $B$ of the triggering load. Numerical results presented below and by *Gomberg et al.* [1997] demonstrate this to be true for transient loads applied throughout the earthquake cycle. Consequently, Coulomb failure model predictions differ significantly from those which account for rock physics embodied in rate-and-state friction relations. For example, Coulomb failure models predict no change in the time of failure ($\Delta t = 0$) for any transient load (Figure 1) (except when it raises the stress to the threshold stress level, in which case failure occurs during the transient, so that for short-duration transients $\Delta t$ is essentially single-valued or $\Delta t = t_f - t_0$). The numerical rate-and-state modeling experiments of *Gomberg et al.* [1997] showed that a small-amplitude transient load, even an oscillating load, may bring a fault closer to failure. This is because of the logarithmic dependence of the friction on rate and state and because the state evolution equation (3) implies a competition between a bounded healing rate and an unbounded weakening rate.

The relationship between $\Delta t$ and $t_0$ predicted by (12) differs for the transient and static loads. This difference has implications not only for their effects on the timing of triggered earthquakes but also for the stresses required for failure. For both types of triggering loads the delay (failure time minus $t_0$) decreases the later the load is applied (Figure 3). For a transient load, $\Delta t$ increases with increasing $t_0$ (Figure 3a), while for a static load the opposite is true: $\Delta t$ decreases with increasing $t_0$ (Figure 3b). (Thus a stress step imposed late in the earthquake cycle causes less clock advance than an equivalent step imposed earlier.) This contrast appears to be independent of the specific form of the transient, as suggested by similar re-

sults for oscillating transients in the numerical study of *Gomberg et al.* [1997]. Note that differentiation of (12) with respect to $t_0$ shows that $d\Delta t/dt_0$ is always positive for the square-wave transient and negative for the step.

The reason for the difference between the responses to static and transient loads may be understood by noting that in the static case, the earlier an additional permanent load is applied the longer the duration over which its effect accumulates (leading to a greater net effect or $\Delta t$). For transients the duration $t_w$ is the same regardless of $t_0$. However, the fault slips more slowly for earlier values of $t_0$ so it takes relatively more time to become unstable when $t_0$ is earlier, resulting in a smaller clock advance [*Gomberg et al.*, 1997]. The differing effects of transient and static loads may be shown explicitly by noting that the velocity (equation (10b)) and clock advance (equation (12)) increase as the load function $L$ increases. $L$ increases for a transient applied later (larger $t_0$). However, $L$ increases for a static load applied earlier (smaller $t_0$). This relationship between $L$ and $t_0$ (Table 2) and the relationship between the transient and static load become clear by considering the static load function as a sum of transients. Applying a static load earlier and thus for a longer time is equivalent to adding more transients so that a larger $L$ and a greater clock advance result. This is demonstrated mathematically in the appendix.

The relationships between $t_0$ and $\Delta t$ also have significant implications for the stresses required for failure. The rate-and-state-based relationships imply that a constant amplitude stress failure threshold does not exist, while such a threshold is implicit in Coulomb failure models (Figure 1). Instead, the frictional instability model predicts that the stress amplitude at the time of failure depends on the loading history. Numerical calculations illustrate a crucial difference between frictional instability and Coulomb failure models (Figure 4). For instability models and static loads the stress at failure will be less than the background-only value when $t_0$ is small and may exceed it for loads applied late in the cycle (Figure 4a). For transient loads the stress at failure will always be less than it would have been without any triggering load, whereas in the Coulomb failure model a transient has no effect on the stress at the time of failure (Figure 1).

The clock advance in the rate-and-state model determines the failure time and thus the peak stress at failure. A variable stress at failure results from (1) the dependence of $\Delta t$ on $t_0$, (2) the proportionality between stress and load displacement which follows from equation (1), and (3) the fact that the slip at failure is constant and equal to $x_f$ (equation (13)). All these factors imply that in the absence of a triggering load, from equation (1) evaluated at $t = t_f$, the stress on the fault at failure equals

$$\tau_f = \sigma_n k[x_{\mathrm{lp}}(t_f) - x_f] = \sigma_n k[V_b t_f - x_f] \tag{14a}$$

(Recall that $t_f$ (equation (11)) is the failure time in the absence of a triggering load.) When a static load of amplitude $\sigma_n k \Delta x_{lp}$ is applied at $t = t_0$, the stress at failure equals

$$\begin{aligned}\tau_{\mathrm{static}} &= \sigma_n k[x_{\mathrm{lp}}(t_f - \Delta t) - x_f] \\ &= \sigma_n k\{V_b t_0 + \Delta x_{\mathrm{lp}} + V_b[t_f - t_0 - \Delta t] - x_f\} \\ &= \sigma_n k\{V_b[t_f - \Delta t] + \Delta x_{\mathrm{lp}} - x_f\}\end{aligned} \tag{14b}$$

Thus, differencing (14a) and (14b) shows that a static triggering load changes the failure stress by

$$\Delta\tau_{\mathrm{static}} = \sigma_n k[\Delta x_{\mathrm{lp}} - V_b \Delta t] \tag{15a}$$

A transient triggering load only lasts for a short duration so that the change in stress at failure is

$$\Delta\tau_{\mathrm{transient}} = -\sigma_n k V_b \Delta t \tag{15b}$$

Equations (15) demonstrate that the change in failure stress due to a triggering load is proportional to the clock advance, that for a transient load the stress at failure will always be less than it would have been without any triggering load, and that for a static load it may be larger or smaller depending on the relative sizes of $\Delta x_{\mathrm{lp}}$ and $V_b \Delta t$. For transient loads the failure stress is smaller the later it is applied because $\Delta t$ is greater for later values of $t_0$. For static loads applied early, $\Delta t$ will be greater than $\Delta x_{\mathrm{lp}}/V_b$ and the failure stress will be less than the background-only value. However, late in the cycle $\Delta t$ becomes smaller than $\Delta x_{\mathrm{lp}}/V_b$ and the stress at failure may actually exceed the background-only value (Figure 4a). Note that $\Delta\tau_{\mathrm{transient}}$ and $\Delta\tau_{\mathrm{static}}$ are not equivalent to ΔCFSs which describe the change in the Coulomb stress acting on a fault; instead, they describe the change in failure stress, which is constant for the Coulomb model.

The predictions of the rate-and-state and Coulomb failure models for static stress steps are compared in Figure 5, in which we plot the failure time as a function of $t_0$. For the Coulomb failure model, $\Delta t$ is a constant until $t_0$ equals or exceeds the clock-advanced failure time, beyond which triggering becomes instantaneous. The Coulomb failure model underpredicts $\Delta t$ for triggering loads applied early in the cycle and overpredicts it late in the cycle compared to the numerical rate-and-state calculations (Figure 5). In the example shown which uses the parameters in Table 1, after 55% and 85% of the cycle has elapsed, the Coulomb prediction differs from the rate-and-state value by −26% and +36%, respectively.

Figure 5 also illustrates the accuracy of the approximate closed-form equations with respect to $t_0$. The analytically calculated clock advance always underpredicts the full solution to the rate-and-state equations. In the example shown in Figure 5 this error is small for large values of $t_0$; e.g., at 85% of the cycle time the analytic prediction is in error by 10%. It exceeds 30% when $t_0$ occurs before 55% of the cycle has elapsed. Although the error depends on the model parameters, this and other examples demonstrate that caution should be exercised when using these approximate equations to predict the clock advance. Note also that the relationships illustrated in Figures 4 and 5 and discussed above are specific to the evolution equation (3) we have used. The variation of $\Delta t$ with $t_0$ may differ considerably for other evolution equations proposed in the literature [*Rüina*, 1983]. We chose (3) because it properly accounts for the healing required by experimental observations (i.e., $\xi$ increases with the time of stationary contact) [*Dieterich*, 1979; *Dieterich and Kilgore*, 1994; *Beeler et al.*, 1994], because it has been widely utilized and studied and because it permits the approximations that lead to closed-form equations (12).

Equation (12) can be used to assess the relative potency of coseismic static stress changes and of transient loads, such as those due to seismic waves, to alter earthquake timing. Estimated ratios of peak transient to static stresses from the Landers earthquake range between 48 and 200 at distances of 165–740 km (Table 3) [*Hill et al.*, 1993; *Gomberg*, 1996; *Gomberg and Davis*, 1996]. Except for a lack of seismicity at Parkfield, California, these estimates correspond to sites where seismicity rates increased after the Landers earthquake. Similar ratios are obtained from theoretical calculations of transient and static stresses from the Landers earthquake at distances of

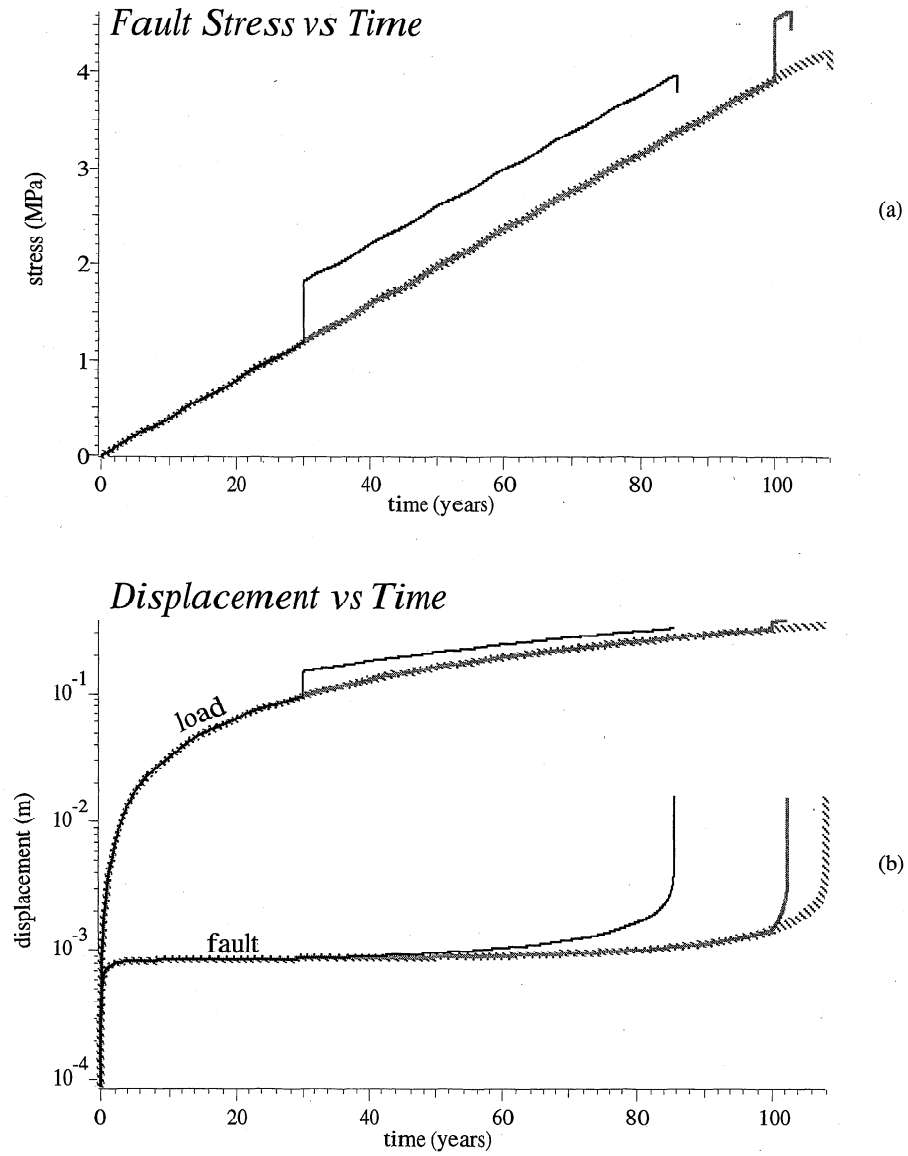


**Figure 4.** Numerical calculations of (a) the fault stress and (b) displacements on a fault under a constant background loading and when subjected to step (static) triggering loads. Examples are shown for triggering load amplitudes of 0.625 MPa applied at $t_0$ = 30 years (thin solid curves) and 100 years (shaded curves), and for only background loading (striped curves) for which $t_f$ = 108.06 years. Model parameters are listed in Table 1. Note that at the time of failure the fault displacement is constant and the stress at failure is lower and higher than the background-only value for triggering loads applied at $t_0$ = 30 years and $t_0$ = 100 years, respectively. Also note that the clock advance is smaller for the load applied at $t_0$ = 100 years than at $t_0$ = 30 years.

10–100 km [*Cotton and Coutant*, 1997]. We assume static and transient stresses may be represented by step and square-wave time functions and calculate $\Delta t$ for a range of load amplitudes and step function durations using (12). Our approximate closed-form expressions predict ratios of transient to static load amplitudes consistent with the aforementioned studies for triggering loads applied in the latter ~10% of the failure cycle. For example, a ratio equal to 64 is predicted for $t_0$ = 107 years; that is, a square wave amplitude of 5.0 MPa and duration of $t_w$ = 200 s will cause an equal clock advance as a step load of ~0.078 MPa (Figure 6). Consistency is poorer when the triggering load is applied earlier in the cycle because the ratio between transient and static load amplitudes required to effect equal clock advance becomes very large. This is because as $t_0$ decreases, $\Delta t$ increases for static loads and decreases for transient loads. The agreement between our estimates with the aforementioned ratios suggests that some natural static and transient triggering is consistent with the frictional instability model (noting that we have neglected any changes in normal stress). The transient to static amplitude ratios also suggest that transient triggering is more likely for faults that are close to failure. We may derive from (12) and Table 2 a general expression describing the amplitudes and durations for which the clock advances from transient (square wave) and static (step) loads will be equal. This expression may be simplified for loads applied late in the cycle and for static stress changes of

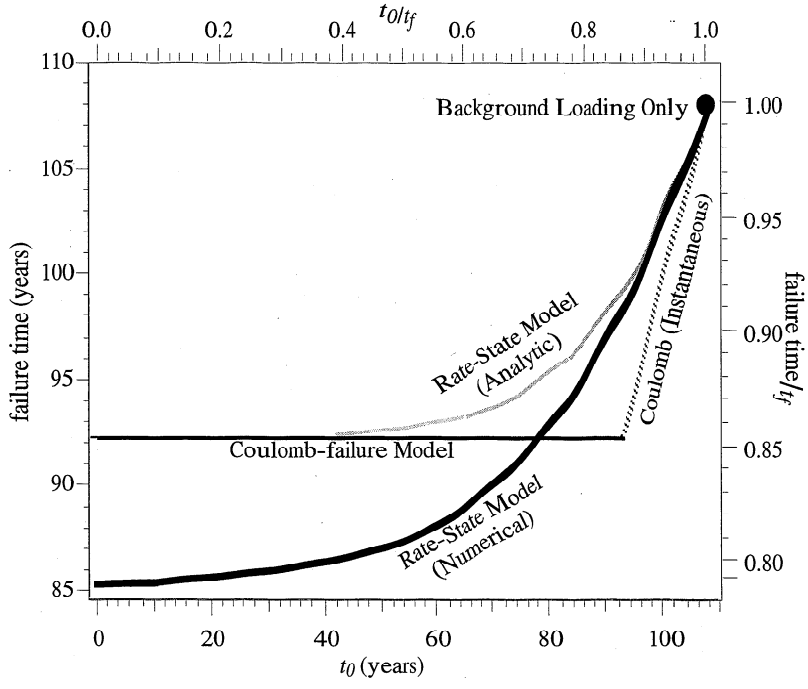


**Figure 5.** Failure time as a function of the time $t_0$ that a static shear triggering load of 0.625 MPa is applied. Numerical model (thick solid curve) calculations use parameters in Table 1. Predictions of the closed-form equations (12) (shaded curve) are calculated using the same parameters described in Figure 2 for a single static load of 0.625 MPa. The clock advance $\Delta t$ equals the difference between the failure time and $t_f = 108.06$ years. $\Delta t = 15.9$ years for the Coulomb failure model and is independent of $t_0$ (thin solid line), until $t_0 \geq t_f - \Delta t$, when triggering becomes instantaneous (thin striped line).

the order of several hundredths megapascals, of the same order as those inferred to correlate with increased seismicity rates. When these criteria are met, $\dot{\mu}_b(t_f - t_0)/a \ll 1$ and $B_{st}/a \ll 1$ and the square wave and step amplitudes that result in approximately equal clock advances satisfy

$$B_{\text{transient}} \sim a \ln \{[(t_f - t_0)/t_w](B_{\text{static}}/a)\} \quad (16)$$

For example, the transient amplitude must be an order of several hundred times greater than the static value for values appropriate to faulting (i.e., $\Delta\tau_{\text{transient}}/\Delta\tau_{\text{static}} = B_{\text{transient}}/B_{\text{static}} = 179$ if $t_w \sim 1000$ s, $(t_f - t_0) \approx 1$ year, $\Delta\tau_{\text{static}} = \sigma_n B_{\text{static}} = 0.020$ MPa, $a = 0.005$, then $\Delta\tau_{\text{transient}} = \sigma_n B_{\text{transient}} = 3.57$ MPa). Note that the absolute amplitudes of both the modeled static and transient loads needed to generate clock advances of the order of a year or more exceed those observed by approximately an order of magnitude (e.g., from Figure 6, $\Delta t \approx 300$ days when $\Delta\tau_{\text{static}} \approx 0.6$ MPa and $\Delta\tau_{\text{transient}} \approx 5.0$ MPa, $t_w = 1000$ s for $t_0 = 107$ years). Although better agreement would clearly be more satisfying, these calculations are based on constitutive parameters measured in laboratory experiments at room temperature and short timescales; it is likely that the relevant parameters differ for real earthquake processes. In addition, a simple spring and slider block model clearly cannot account for the complexity of the real earthquake rupture process.

**Table 3.** Static and Transient Stress Change Estimates, Landers Earthquake

| Site | Distance, km | Static, MPa | Transient, MPa | Transient/Static |
|---|---|---|---|---|
| Indian Wells | 165–205 | 0.002–0.006 | 0.8 | 133–200 |
| Little Skull Mountain | 240 | 0.0028 | 0.2 | 72 |
| Parkfield | 410 | 0.00069 | 0.15 | 217 |
| Geysers | 740 | 0.00087 | 0.042 | 48 |

Estimates of changes in coseismic static [*Hill et al.*, 1993] and transient [*Gomberg*, 1996; *Gomberg and Davis*, 1996] stress changes caused by the Landers earthquake. Seismicity increases were observed at all sites except at Parkfield.

Equation (12) also allows us to examine the relationship between triggering load amplitude and clock advance, noting that a linear scaling between these is implicit in many studies that invoke the Coulomb failure model [*Harris and Simpson*, 1992, 1996; *Stein et al.*, 1992; *King et al.*, 1994; *Nostro et al.*, 1997; *Deng and Sykes*, 1997; *Pollitz and Sacks*, 1997]. Figure 7 plots $\Delta t$ as a function of load amplitude $\Delta\tau$. As in Figure 5, Figure 7b shows that the assumed linear scaling overpredicts the clock advance. Equation (12) and Table 2 describe the relationship between clock advance and triggering load amplitude and show that larger loads lead to greater clock advances. However, as (12) and Figure 7b show, $\Delta t$ only scales linearly with the load amplitude for the step function load when it has small amplitude. When $B_{st}/a = (\Delta\tau/a\sigma_n)$ is small, the step function clock advance becomes

$$\Delta t \sim [B_{st}/\dot{\mu}_b] = [\Delta\tau/\dot{\tau}_b] \quad (17)$$

The closed-form equations (12) also show that $\Delta t$ for the square wave is much smaller because its corresponding load function $L$ is smaller by a factor approximately equal to $\dot{\mu}_b t_{w/a}$ (Table 2) and because it lacks the linear term (i.e., $B_{st} = 0$) that leads to the linear scaling. Note that (17) also is mathe-

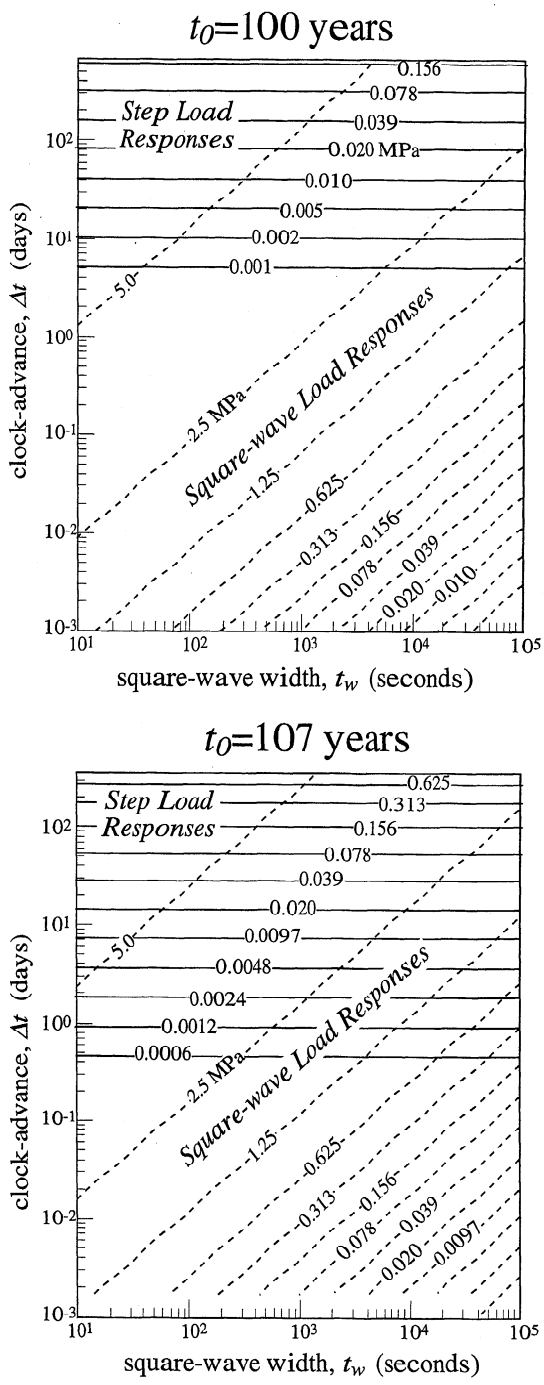


**Figure 6.** Comparisons of the clock advances resulting from static and transient loads applied at (top) $t_0$ = 100 years and (bottom) $t_0$ = 107 years. The cycle time in the absence of a triggering load is 108.06 years. Dashed lines show the relationship between clock advance $\Delta t$ and transient duration $t_w$ predicted by (12) for different amplitude (MPa) square wave loads. Solid lines show $\Delta t$ predicted for various step load amplitudes (MPa). The model parameters used are the same as in Figure 2. Results plotted in Figure 5 suggest that these calculations should differ from the full numerical solution by <10%.

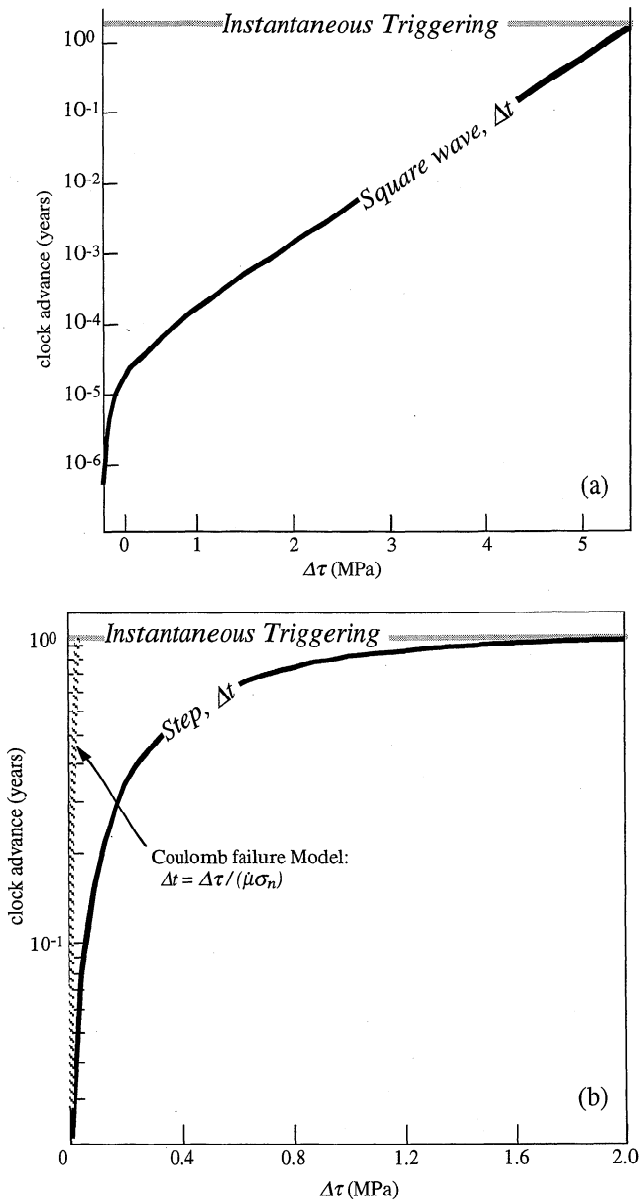


**Figure 7.** Clock advances $\Delta t$ predicted by (12) and Table 2 for varying load amplitudes (thick curves) at $t_0$ = 107 years. The shaded horizontal lines indicate the maximum clock advance or when instability occurs instantaneously upon application of the triggering load. See Figure 2 for initial conditions. (a) Results for a square-wave load with duration $t_w$ = 1000 s. (b) Results for a step load. The striped curve shows $\Delta t$ assuming it scales linearly with the load amplitude as in Coulomb failure models. Note that the axes differ in Figures 7a and 7b.

matically true for small $t_0$, but the closed-form expressions are not valid in such cases. Numerical calculations shown in Figure 5 show that the approximate solutions become equal to the Coulomb failure model predictions at small $t_0$; however, they are inconsistent with the more accurate numerical solutions.

## 4. Discussion: Triggering Effects on Earthquake Populations, New Earthquakes

Thus far we have considered the effect of triggering loads on a single fault, but in practice, it may difficult to isolate the effect of stress history on a single fault generating repeating earthquakes, analogous to our spring and slider block model. A more tractable test of rate-and-state predictions may be the response of earthquake populations to changes in stress which may be revealed in changes in seismicity rate [*Reasenberg and Simpson*, 1992; *Dieterich*, 1994; *Stein et al.*, 1997; *Toda et al.*, this issue]. We now summarize some of the observations that

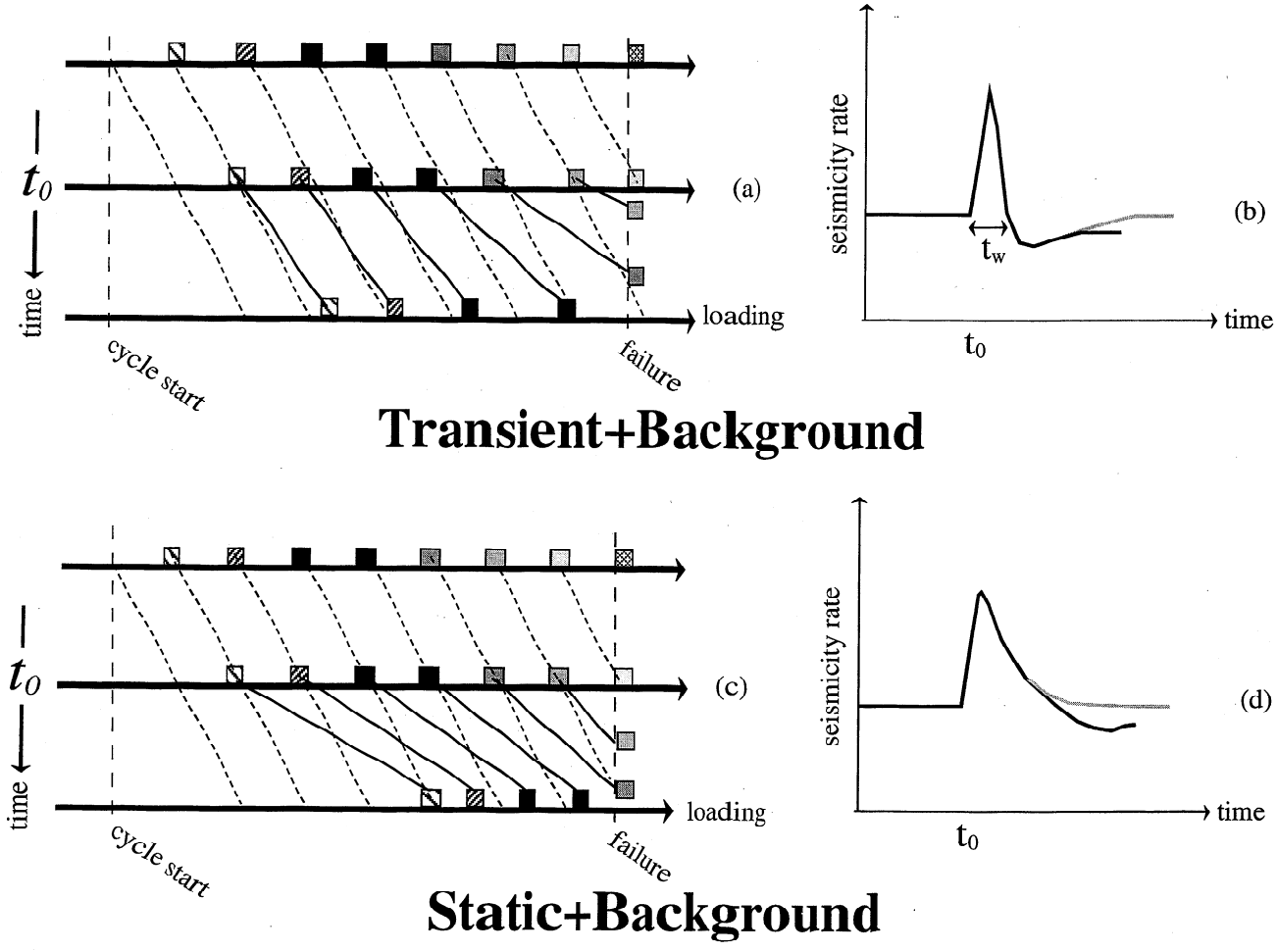


**Figure 8.** Schematic illustration of the effect of clock advances on a population of earthquakes for a background load plus a transient (Figures 8a and 8b) or static (Figures 8c and 8d) load. (a) and (c) Each block represents a fault at a different stage in the loading cycle and each row represents an instant in time. At the constant background loading rate the faults would be loaded along the dashed lines, so that one fault fails per unit of time. If a transient triggering load is applied at $t_0$ (middle row), the loading process is clock advanced as shown by the solid lines. For either the transient or static load, there is an initial increase in the number of faults that fail (represented by blocks that have crossed the vertical failure line). However, for the transient load the remaining faults are now farther apart in their loading cycle (represented by wider spacing between blocks on a row), and for the static case they are closer together (see Figure 3). (b) For the transient load the increase in seismicity rate cannot last longer than the transient duration $t_w$, and the rate later decreases to below the background rate. (d) The increased rate persists longer for the static load (blocks/faults are now more closely spaced in the loading cycle). The seismicity rate following the rate increase and transient quiescence depends strongly on how the system is "recharged"; i.e., whether the site labeled "cycle start" is filled with faults that just failed or from some reservoir of available faults. In figures 8b and 8d, in the case with no recharge, the seismicity rate will experience a quiescence for both the static and transient loads (solid curve) and the pattern of seismicity repeats until another triggering load perturbs it again. In the case with recharge, the seismicity rate will return to the background rate (shaded curve).

may help to discriminate between two models of earthquake triggering. In one model, triggered earthquakes are those with failure times advanced by the triggering load (i.e., clock advanced). Alternatively, triggered earthquakes may be "new," that is, ones that would not have occurred in the absence of the triggering load [*Gomberg et al.*, 1997]. We conclude below that neither model may be rejected using existing seismicity data. However, these hypotheses may be testable in the laboratory or perhaps with real earthquake data as yet uncollected.

To date, evidence of both near- and far-field triggering has been identified by periods of increased seismicity rates which have durations that significantly exceed those of possibly causative transients such as seismic waves. The duration of this increase and whether it is followed by a return to the background rate or a quiescence might serve to illuminate the characteristics of fault populations and triggering loads. For example, consider a fault population in which earthquakes occur at constant rate under background loading. Figure 8 illustrates schematically the possible effects on seismicity rates on such a population, of superposing a transient or static load. The effects of either triggering load are to cause some faults to fail immediately and bring others closer to failure (i.e., cause clock advance). For any type of triggering load the evolution of seismicity rates depends strongly on whether the population of

seismogenic faults is finite or effectively infinite. For a finite population of faults an increased earthquake rate leaves fewer faults available for failure and thus a quiescence follows a seismicity increase (Figure 8d, solid curve). However, for a sufficiently large reservoir of available faults subjected to a stress step, no quiescence results because those faults that failed during the period of increased seismicity need not be reloaded for the seismicity rate to return to the background level (Figure 8d, shaded curve). The assumption of an essentially infinite population is implicit in the modeling of aftershock seismicity by *Dieterich* [1994] and seems reasonable for small magnitude earthquakes. However, above some magnitude level the population of available faults must be finite, although rates of earthquakes become more difficult to estimate. A quiescence results from a transient load for either a finite or infinite fault population because the clock advance is greater for earthquakes farther along in their loading cycle (see Figures 8a and 8b). A quiescence results from a static load only for a finite fault population (see Figures 8c and 8d). Thus a quiescence is only consistent with a model in which triggered earthquakes are events that are clock advanced by static stress changes on a finite set of available faults or by stress transients on any fault population. We also note that the rate-and-state clock advance model predicts that the duration of increased seismicity cannot exceed the duration of the triggering transient load (Figure 8a). These characteristics might permit us to distinguish between static and transient triggering (e.g., as in work by *Dieterich* [1993]), assuming that triggering simply alters the timing of earthquakes.

In a number of observational studies, rate increases are followed directly by a return to the background rate. For example, *Dieterich* [1994] finds that seismicity rates during and following a number of aftershock sequences may be fit with functions that quickly return from elevated values to the background value. Indeed, many aftershock sequences may be described by Omori's law, in which the immediate increase in numbers of earthquakes decays hyperbolically with time to the background rate. Albeit qualitative, evidence cited by *Gomberg and Davis* [1996] does not indicate any quiescence following both aftershock and remotely triggered earthquake sequences at The Geysers, California. Remotely triggered earthquakes at Long Valley, California, occurred in excess of the background at a statistically significant level [*Hill et al.*, 1995], with no subsequent quiescence. In contrast, *Jones and Hauksson* [1997] detected quiescences following seismicity increases (for $M > 3.0$ events) after the two largest earthquakes in historic times in southern California. Assessing whether quiescence is relatively less common is difficult, as the signal in a quiescent period is more difficult to observe because it is bounded (i.e., the seismicity rate cannot be less than zero). Thus it may require assessing statistical significance for a small number of data, particularly in regions of low background seismicity rates.

An alternative interpretation of seismicity data relevant to triggering is that some or all of the triggered earthquakes are actually new. New earthquakes may be dormant faults which are activated by a change in stress orientation associated with the triggering load [*Michael*, 1987]. New earthquakes might also be existing active faults which creep in a "conditionally stable" fashion in response to the background loading but slide unstably when perturbed (see *Boatwright and Cocco* [1996] and *Gomberg et al.* [1997] for discussions of plausible new earthquake models). If new earthquakes are generated by the triggering load, those events appear as excess events above the background population. In this case, increases in seismicity rates caused by static or transient loading need not be followed by quiescences. In addition, if transient triggering of new earthquakes occurs with some delay the period of increased seismicity rate may exceed the duration of the transient. Therefore the presence of new earthquakes would not allow finite or infinite populations and the type of triggering load to be distinguished from one another (i.e., a lack of quiescence and the duration of rate changes are no longer distinguishing features).

## 5. Conclusions

Observational evidence for both static and transient near- and far-field triggering may be explained in terms of a frictional instability model, where the fault obeys rate-and-state dependent frictional constitutive relations, as has been invoked in previous studies to explain other aspects of the earthquake cycle. We assume the normal stress to be constant. Simple stress history changes or triggering loads added to a constant stressing rate, consist of square-wave transients representing seismic waves or stress steps representing static stress increases. These changes lead to reduction in the failure time, defining a clock advance relative to the failure time in the absence of the triggering loads. Assuming a simplified form of state variable, as advocated by *Dieterich* [1992], analytical solutions for single square-wave and step loads can be developed. The approximate closed-form equations we derive following *Dieterich* [1992, 1994], also have been used to evaluate the affect of static stress changes on seismicity rates [e.g., *Toda et al.*, this issue] and single earthquakes [see *Harris and Simpson*, this issue]. We expand on the work by *Dieterich* [1992, 1994] and develop closed-form equations for transient loads.

Calculations based on this closed-form approximate formulation and full solutions calculated numerically show that clock advance is a complex function of the load characteristics. The transient amplitude must be several hundred times greater than the static value to cause equal clock advance, consistent with observational and theoretical evidence. The relationship between clock advance $\Delta t$ and the time the triggering load is applied, $t_0$, differs for the transient and static loads. A static load imposed late in the earthquake cycle causes less clock advance than an equal load imposed earlier. For a transient load the opposite is true; $\Delta t$ increases with increasing $t_0$. This dependence of $\Delta t$ on $t_0$ has implications for the stresses required for failure; for transient loads the stress at failure will always be less than it would have been without any triggering load. This may also be true for static loads, and it is also possible for the failure stress to exceed the background-only value. Another consequence of the rate-and-state model is that the total slip at failure is a constant for any given set of model parameters. Thus triggering thresholds correspond to a maximum slip. The accuracy of the closed-form solution to the rate-and-state equations differs from the full solution as a function of $t_0$, always underpredicting the clock advance. The difference is $\sim$10% at 85% of the cycle time and may exceed 30% when $t_0$ occurs before 55% of the cycle has elapsed.

Coulomb failure predictions generally differ significantly from those based on rate-and-state friction. Unlike the rich variation in $\Delta t$ as a function of $t_0$ predicted by the latter, Coulomb failure models predict that $\Delta t$ equals the amplitude of the static stress change divided by the background loading rate. In comparison to the rate-and-state model the Coulomb failure model underpredicts $\Delta t$ for triggering loads applied

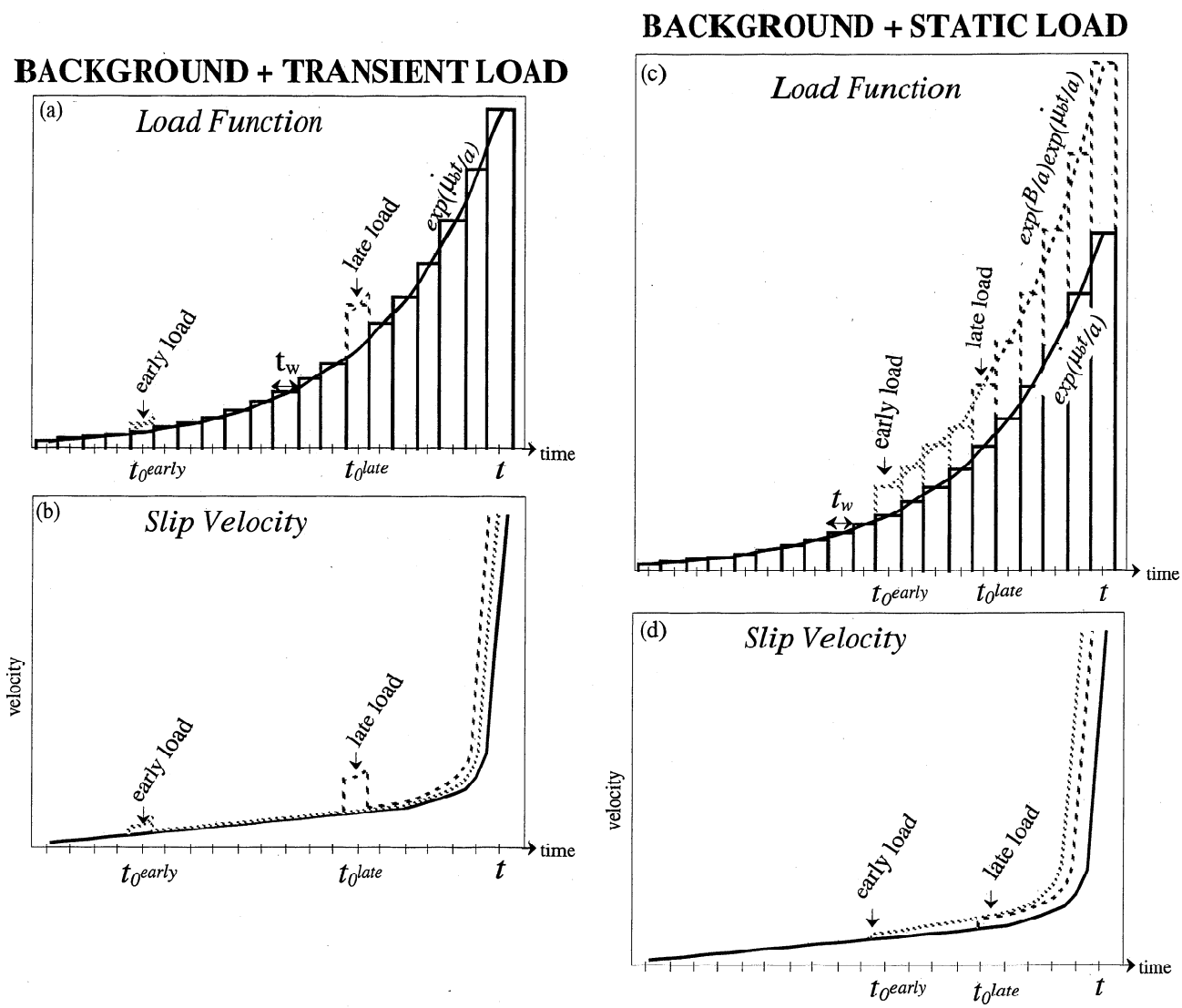


**Figure A1.** Schematic illustration of equations (A1) and (A2) for (a) the transient and (c) static load functions $L$ and (b) and (d) how the corresponding velocities evolve with time. Square waves represent transients, or equivalently the numerical form of the integral that constrains $L$ (i.e., equals exp $(B/a)$ exp $(\dot{\mu}_b t/a)$ + $L$). The closed-form solution is shown by the solid curves; the effect of the triggering load is to scale the amplitude of the background load by a factor of exp $(B/a)$. Results for later applied loads are shown by longer dashed curves, earlier ones by shorter dashed (shorter plus longer for the static load function) curves, and solid curves for a background load only. These figures are schematic in order to permit the relevant responses to be shown on a single figure (acceleration to instability takes years, while transients last several hours at most). However, all the features of these figures are based on actual calculations.

early in the cycle and overpredicts it late in the cycle. For the Coulomb failure model, $\Delta t = 0$ for any transient load, whereas $\Delta t > 0$ for the rate-and-state model. Finally, instead of a slip failure threshold, a constant amplitude stress failure threshold is implicit in Coulomb models.

Determining the effect of stress perturbation on a population of faults obeying rate-and-state friction relations to match observed changes in seismicity rate is not straightforward because it requires assumptions about population characteristics. If triggering is equivalent to causing clock advance then its effect on seismicity rates will depend on whether the population of faults is finite or is effectively infinite (as *Dieterich* [1994] assumes). In addition, the duration of increased seismicity triggered by a transient cannot exceed the transient's duration. Seismicity characteristics such as quiescences and the duration of rate changes may distinguish between characteristics of fault population size and triggering load types. However, seismicity data can no longer distinguish between these if an alternative view is adopted, that is, that triggered earthquakes are actually "new" (would not have happened in the absence of the triggering load).

We conclude that both static and transient deformation changes may hasten the occurrence of future earthquakes. At near-field distances, within the traditionally recognized aftershock zone, both seismic wave transients and static coseismic changes may induce instabilities with variable time delays. At remote distances, only seismic wave transients have sufficient energy to cause the changes that result in local slip instabilities. To the extent that earthquakes may be characterized as frictional instabilities, the evidence we present clarifies the chal-

lenge of deterministic time predictability of most earthquakes. In order to predict the time of an earthquake successfully, we now must know, and properly account for, the fault's slip history and the applied loads it has experienced.

## Appendix

The relationships between $L$ and $t_0$ (Table 2) for transient and static loads may be understood by considering the static load function to be a sum of transients. This can be seen by first separating the right side of (8) (describing the temporal response) into three intervals. These correspond to the interval prior to the application of the triggering load, to the duration of a transient, and to the remaining time when a static load may be imposed, as follows:

$$\int_0^t \exp\left(\frac{[\dot{\mu}_b t' + Bf(t')]}{a}\right) dt'$$

$$= \int_0^{t_0} \exp\left(\frac{\dot{\mu}_b t'}{a}\right) dt' + \exp\left(\frac{B}{a}\right) \int_{t_0}^{t_0+t_w} \exp\left(\frac{\dot{\mu}_b t'}{a}\right) dt'$$

$$+ \exp\left(\frac{B_{st}}{a}\right) \int_{t_0+t_w}^{t} \exp\left(\frac{\dot{\mu}_b t'}{a}\right) dt' \qquad \text{(A1)}$$

$B_{st} = 0$ for the square-wave load, and $B = 0$ and $B_{st} = 0$ for a background load only. We use the approximations that $\exp(\dot{\mu}_b t_w/a) - 1 \approx (\dot{\mu}_b t_w/a)$ and that the durations prior to $t_0$ (first right-side integral of (A1)) and after $t_0 + t_w$ (third right-side integral) may be divided into $M$ and $N$ intervals of widths $t_w$, respectively. The integrals of (A1) may then be written as sums (equivalent to evaluating them numerically) as

$$\int_0^t \exp\left(\frac{[\dot{\mu}_b t' + Bf(t')]}{a}\right) dt'$$

$$\approx t_w \left\{ \sum_{m=0}^{M-1} \exp\left(\frac{m\dot{\mu}_b t_w}{a}\right) + \exp\left(\frac{B}{a}\right) \exp\left(\frac{\dot{\mu}_b t_0}{a}\right) \right.$$

$$\left. + \exp\left(\frac{B_{st}}{a}\right) \exp\left(\frac{\dot{\mu}_b t_0}{a}\right) \sum_{n=1}^{N-1} \exp\left(\frac{n\dot{\mu}_b t_w}{a}\right) \right\} \qquad \text{(A2)}$$

Figures A1a and A1c graph expressions (A1) and (A2) schematically for both the transient and static loads, and Figures A1b and A1d show how the corresponding velocities evolve with time. The effect of a transient load on its $L$ is to scale the amplitude of the background load during the time it is applied by a factor of $\exp(B/a)$. Therefore, because the background load grows with time, the transient $L$ will be increased by a greater amount the later the transient is applied. A later transient thus leads to a larger clock advance (Figures A1a and A1b). Equation (A2) shows that the static load function may be considered as a sum of transient contributions. Applying a static load earlier (and thus for a longer time) is equivalent to adding more transients such that a larger static $L$ and a greater clock advance result (Figures A1c and A1d).

**Acknowledgments.** The authors would like to thank A. McGarr, P. Reasenberg, R. Harris, M. Cocco, K. Rybicki, and an anonymous reviewer for their thoughtful and helpful reviews. They also thank Jim Dieterich and Brian Kilgore for helpful discussions and suggestions. CERI contribution 348.

## References

Anderson, J. G., J. N. Brune, J. N. Louie, Y. Zeng, M. Savage, G. Yu, Q. Chen, and D. dePolo, Seismicity in the western Great Basin apparently triggered by the Landers, California, earthquake, 28 June 1992, *Bull. Seismol. Soc. Am., 84,* 863–891, 1994.

Beeler, N. M., T. E. Tullis, and J. D. Weeks, The roles of time and displacement in the evolution effect in rock friction, *Geophys. Res. Lett., 21,* 1987–1990, 1994.

Boatwright, J., and M. Cocco, Frictional constraints on crustal faulting, *J. Geophys. Res., 101,* 13895–13910, 1996.

Bodin, P., and J. Gomberg, Triggered seismicity and deformation between the Landers, California, and Little Skull Mountain, Nevada, earthquakes, *Bull. Seismol. Soc. Am., 84,* 835–843, 1994.

Brace, W. F., and J. D. Byerlee, Stick-slip as a mechanism for earthquakes, *Science, 153,* 990–992, 1966.

Caskey, S. J., and S. G. Wesnousky, Static stress changes and earthquake triggering during the 1954 Fairview Peak and Dixie Valley earthquakes, central Nevada, *Bull. Seismol. Soc. Am., 87,* 521–527, 1997.

Cotton, F., and O. Coutant, Dynamic stress variations due to shear faults in a plane-layered medium, *Geophys. J. Int., 128,* 676–688, 1997.

Deng, J., and L. R. Sykes, Evolution of the stress field in southern California and triggering of moderate-size earthquakes: A 200-year perspective, *J. Geophys. Res., 102,* 9859–9886, 1997.

Dieterich, J. H., Time-dependent friction in rocks, *J. Geophys. Res., 77,* 3690–3697, 1972.

Dieterich, J. H., Time-dependent friction and the mechanics of stick slip, *Pure Appl. Geophys., 116,* 790–806, 1978.

Dieterich, J. H., Modeling of rock friction, 1, Experimental results and constitutive equations, *J. Geophys. Res., 84,* 2161–2168, 1979.

Dieterich, J. H., Constitutive properties of faults with simulated gouge, in *Mechanical Behavior of Crustal Rocks, Geophys. Monogr., Ser.* vol. 24, edited by N. L. Carter et al., pp. 103–120, AGU, Washington, D.C., 1981.

Dieterich, J. H., A model for the nucleation of earthquake slip, in *Earthquake Source Mechanics, Geophys. Monogr. Ser.*, vol. 37, edited by S. Das, J. Boatwright, and C. Scholz, pp. 36–49, AGU, Washington, D.C., 1986.

Dieterich, J. H., Earthquake nucleation on faults with rate- and state-dependent strength, *Tectonophysics, 211,* 115–134, 1992.

Dieterich, J. H., Simulation of earthquake triggering, *Eos Trans. AGU,* 74 (16), Spring Meet. Suppl., 317–318, 1993.

Dieterich, J., A constitutive law for rate of earthquake production and its application to earthquake clustering. *J. Geophys. Res., 99,* 2601–2618, 1994.

Dieterich, J. H., and B. D. Kilgore, Direct observation of frictional contacts: New insights for state-dependent properties, *Pure Appl. Geophys., 143,* 283–302, 1994.

Gomberg, J., Stress/strain changes and triggered seismicity following the $M_w$7.3 Landers, California, earthquake, *J. Geophys. Res., 101,* 751–764, 1996.

Gomberg, J., and P. Bodin, Triggering of the Little Skull Mountain, Nevada earthquake with dynamic strains, *Bull. Seismol. Soc. Am., 84,* 844–853, 1994.

Gomberg, J., and S. Davis, Stress/strain changes and triggered seismicity at The Geysers, California, *J. Geophys. Res., 101,* 733–750, 1996.

Gomberg, J., M. L. Blanpied, and N. M. Beeler, Transient triggering of near and distant earthquakes, *Bull. Seismol. Soc. Am., 87,* 294–309, 1997.

Gu, Y., and T. Wong, Effects of loading velocity, stiffness, and inertia on the dynamics of a single degree of freedom spring-slider system, *J. Geophys. Res., 96,* 21677–21691, 1991.

Gu, J., J. R. Rice, A. L. Ruina, and S. T. Tse, Slip motion and stability of a single degree of freedom elastic system with rate and state dependent friction, *J. Mech. Phys. Solids, 32,* 167–196, 1984.

Harris, R. A., Introduction to special section: Stress triggers, stress shadows, and implications for seismic hazard, *J. Geophys. Res.,* this issue.

Harris, R., and R. W. Simpson, Changes in static stress on southern California faults after the 1992 Landers earthquake, *Nature, 360,* 313–318, 1992.

Harris, R., and R. W. Simpson, In the shadow of 1857: Effect of the great Ft. Tejon earthquake on subsequent earthquakes in southern California, *Geophys. Res. Lett., 23,* 229–232, 1996.

Harris, R., and R. W. Simpson, Suppression of large earthquakes by stress shadows: A comparison of Coulomb and rate-and-state friction laws, *J. Geophys. Res.,* this issue.

Harris, R., R. W. Simpson, and P. A. Reasenberg, Influence of static stress changes on earthquake locations in southern California, *Nature, 385,* 221–224, 1995.

Hill, D. P., et al., Seismicity remotely triggered by the magnitude 7.3 Landers, California, earthquake, *Science, 260,* 1617–1623, 1993.

Hill, D. P., M. J. S. Johnston, and J. O. Langbein, Response of Long Valley caldera to the $M_w$ = 7.3 Landers, California, earthquake, *J. Geophys. Res., 100,* 12985–13005, 1995.

Hodgkinson, K. M., R. S. Stein, and G. Marshall, The 1954 Rainbow Mountain-Fairview Peak-Dixie Valley earthquakes: A triggered normal faulting sequence, *J. Geophys. Res., 101,* 25459–25472, 1996.

Ida, Y., Cohesive force across the tip of a longitudinal shear crack and Griffith's specific surface energy, *J. Geophys. Res., 77,* 3796–3805, 1972.

Jaumé, S. C., and L. R. Sykes, Changes in state of stress on the southern San Andreas fault resulting from the California earthquake sequence of April to June, 1992, *Science, 258,* 1325–1328, 1992.

Jaumé, S. C., and L. R. Sykes, Evolution of moderate seismicity in the San Francisco Bay region, 1850 to 1993: Seismicity changes related to the occurrence of large and great earthquakes, *J. Geophys. Res., 101,* 765–790, 1996.

Jones, L., and E. Hauksson, The seismic cycle in southern California: Precursor or response?, *Geophys. Res. Lett., 24,* 469–472, 1997.

Kagan, Y. Y., and D. D. Jackson, Long-term earthquake clustering, *Geophys. J. Int., 104,* 117–133, 1991.

Kanamori, H., Relation between tectonic stress, great earthquakes, and earthquake swarms, *Tectonophysics, 14,* 1–12, 1972.

Kanamori, H. C., and R. Allen, Earthquake repeat time and average stress drop, in *Earthquake Source Mechanics, Geophys. Monogr., Ser.,* vol. 37, edited by S. Das, J. Boatwright, and C. Scholz, pp. 227–236, AGU, Washington, D.C., 1986.

Keilis-Borok, V. I., and V. G. Kossobokov, Premonitory activation of earthquake flow: Algorithm M8, *J. Earth Planet. Inter., 61,* 73–83, 1990.

King, G. C. P., R. S. Stein, and J. Lin, Static stress changes and the triggering of earthquakes, *Bull. Seismol. Soc. Am., 84,* 935–953, 1994.

Kisslinger, C., A review of theories of mechanisms of induced seismicity, *Eng. Geol., 10,* 85–98, 1976.

Kossobokov, V. G., and J. M. Carlson, Active zone size versus activity: A study of different seismicity patterns in the context of the prediction of algorithm M8, *J. Geophys. Res., 100,* 6431–6441, 1995.

Marone, C., and B. Kilgore, Scaling of the critical slip distance for seismic faulting with shear strain in fault zones, *Nature, 362,* 618–621, 1993.

Marone, C., J. E. Vidale, and W. L. Ellsworth, Fault healing inferred from time dependent variations in source properties of repeating earthquakes, *Geophys. Res. Lett., 22,* 3095–3098, 1995.

Michael, A. J., Stress rotation during the Coalinga aftershock sequence, *J. Geophys. Res., 92,* 7963–7979, 1987.

Nalbant, S. S., A. Hubert, and G. C. P. King, Stress coupling between earthquakes in northwest Turkey and the north Aegean Sea, *J. Geophys. Res.,* this issue.

Newhall, C. G., and E. Dzurisin, Historical unrest at large calderas of the world, *U.S. Geol. Surv. Prof. Pap., 1855,* 1988.

Nostro, C., M. Cocco, and M. E. Belardinelli, Static stress changes in extensional regimes: An application to southern Apennines (Italy), *Bull. Seismol. Soc. Am., 87,* 234–248, 1997.

Nostro, C., R. S. Stein, M. Cocco, and M. E. Belardinelli, Two-way coupling between Vesuvius eruptions and southern Apennine earthquakes, Italy by elastic stress transfer, *J. Geophys. Res.,* this issue.

Okubo, P. G., and J. H. Dieterich, State variable fault constitutive relations for dynamic slip, in *Earthquake Source Mechanics, Geophys. Monogr. Ser.,* vol. 37, edited by S. Das, J. Boatwright, and C. H. Scholz, pp. 25–35, AGU, Washington, D.C., 1986.

Palmer, A. C., and J. R. Rice, The growth of slip surfaces in the progressive failure of over-consolidated clay, *Proc. R. Soc. London Ser. A, 332,* 527–548, 1972.

Pepke, S. L., J. M. Carlson, and B. E. Shaw, Prediction of large events on a dynamical model of a fault, *J. Geophys. Res., 99,* 6769–6788, 1994.

Pollitz, F. F., and I. S. Sacks, The 1995 Kobe, Japan, earthquake: A long-delayed aftershock of the offshore 1944 Tonankai and 1946 Nankaido earthquakes, *Bull. Seismol. Soc. Am., 87,* 1–10, 1997.

Press, F., and C. Allen, Patterns of seismic release in the southern California region, *J. Geophys. Res., 100,* 6421–6430, 1995.

Protti, M., et al., The March 25, 1990 ($M_w$ = 7.0, $M_L$ = 6.8), earthquake at the entrance of the Nicoya Gulf, Costa Rica: Its prior activity, foreshocks, and triggered seismicity, *J. Geophys. Res., 100,* 20345–20358, 1995.

Raleigh, C. B., J. H. Healy, and J. D. Bredehoeft, An experiment in earthquake control at Rangely, Colorado, *Science, 191,* 1230–1237, 1976.

Reasenberg, P. A., and R. W. Simpson, Response of regional seismicity to the static stress change produced by the Loma Prieta earthquake, *Science, 255,* 1687–1690, 1992.

Rice, J., and J. Gu, Earthquake after effects and triggered seismic phenomena, *Pure Appl. Geophys., 121,* 187–219, 1983.

Roy, M., and C. Marone, Earthquake nucleation on model faults with rate-and-state-dependent friction: Effects of intertia, *J. Geophys. Res., 101,* 13919–13932, 1996.

Ruina, A., Slip instability and state variable friction laws, *J. Geophys. Res., 88,* 10359–10370, 1983.

Scholz, C. H., *The Mechanics of Earthquakes and Faulting,* 439 pp., Cambridge Univ. Press, New York, 1990.

Scholz, C. H., Earthquakes and friction laws, *Nature, 391,* 37–42, 1998.

Scholz, C. H., C. A. Aviles, and S. G. Wesnousky, Scale differences between large interplate and intraplate earthquakes, *Bull. Seismol. Soc. Am., 76,* 65–70, 1986.

Seeber, L., J. G. Armbruster, W.-Y. Kim, C. Scharnberger, and N. Barstow, The 1994 Cacoosing Valley earthquakes near Reading, Pennsylvania: A shallow rupture triggered by quarry unloading, *J. Geophys. Res.,* this issue.

Segall, P., and J. R. Rice, Dilatancy, compaction, and slip instability of a fluid-infiltrated fault, *J. Geophys. Res., 100,* 22155–22173, 1995.

Simpson, D. W., Triggered earthquakes, *Annu. Rev. Earth Planet. Sci., 14,* 21–42, 1986.

Singh, S. K., J. G. Anderson, and M. Rodriguez, Triggered seismicity from major Mexican earthquakes, *Bull. Seismol. Soc. Am.,* in press, 1998.

Sleep, N. H., Ductile creep, compaction, and rate and state dependent friction within major fault zones, *J. Geophys. Res., 100,* 13065–13080, 1995.

Sleep, N. H., Application of a unified rate and state friction theory to the mechanics of fault zones with strain localization, *J. Geophys. Res., 102,* 2875–2895, 1997.

Sleep, N. H., and M. L. Blanpied, Creep, compaction, and the weak rheology of major faults, *Nature, 359,* 687–692, 1992.

Spudich, P., L. K. Steck, M. Hellweg, J. B. Fletcher, and L. M. Baker, Transient stresses at Parkfield, California, produced by the *M* 7.4 Landers earthquake of June 28, 1992: Observations from the UPSAR dense seismograph array, *J. Geophys. Res., 100,* 675–690, 1995.

Stark, M. A., and S. D. Davis, Remotely triggered microearthquakes at The Geysers geothermal field, California, *Geophys. Res. Lett., 23,* 945–948, 1996.

Stein, R. S., and M. Lisowski, The 1979 Homestead Valley earthquake sequence, California: Control of aftershocks and postseismic deformation, *J. Geophys. Res., 88,* 6477–6490, 1983.

Stein, R. S., G. C. P. King, and J. Lin, Change in failure stress on the southern San Andreas fault system caused by the 1992 magnitude = 7.4 Landers earthquake, *Science, 258,* 1328–1332, 1992.

Stein, R. S., A. A. Barka, and J. H., Dieterich, Progressive failure on the Northern Anatolian fault since 1939 by earthquake stress triggering, *Geophys. J. Int., 128,* 594–604, 1997.

Sturtevant, B., H. Kanamori, and E. E. Brodsky, Seismic triggering by rectified diffusion in geothermal systems, *J. Geophys. Res., 101,* 25269–25282, 1996.

Toda, S., R. S. Stein, P. A. Reasenberg, J. H. Dieterich, and A. Yoshida, Stress transferred by the 1995 $M_w$ = 6.9 Kobe, Japan, shock: Effect on aftershocks and future earthquake probabilities, *J. Geophys. Res.,* this issue.

Vidale, J. E., W. L. Ellsworth, A. Cole, and C. Marone, Rupture variation with recurrence interval in 18 cycles of a small earthquake, *Nature, 368,* 634–626, 1994.

Vidale, J. E., D. C. Agnew, M. J. S. Johnston, and D. H. Oppenheimer,

Absence of earthquake correlation with Earth tides: An indication of high preseismic fault stress rate, *J. Geophys. Res.*, this issue.

Wong, T., Y. Gu, T. Yanagidani, and Y. Zhao, Stabilization of faulting by cumulative slip, in *Fault Mechanics and Transport Properties in Rocks,* edited by B. Evans and T. Wong, pp. 109–133, Academic, San Diego, Calif., 1992.

N. M. Beeler and M. L. Blanpied, U.S. Geological Survey, 345 Middlefield Road, MS 977, Menlo Park, CA 94025. (e-mail: nbeeler@isdmnl.wr.usgs.gov; mblanpied@isdmnl.wr.usgs.gov)

P. Bodin, Center for Earthquake Research and Information, University of Memphis, Campus Box 526590, Memphis, TN 38152. (e-mail: bodin@ceri.memphis.edu)

J. Gomberg, U.S. Geological Survey, Center for Earthquake Research and Information, University of Memphis, Campus Box 526590, Memphis, TN 38152. (e-mail: gomberg@usgs.gov)

(Received September 3, 1997; revised March 18, 1998; accepted March 31, 1998.)